Table III. Comparison of Lewis Acid Strengths[a]

Lewis acid	Δδ (ppm)	ref
BBr_3	1.49	28a
$AlCl_3$	1.23	28a
$[HC(py)_3W(NO)_2](SbF_6)_2$	1.19	
BF_3	1.17	28a
$[HC(py)_3Mo(NO)_2](SbF_6)_2$	1.05	
$TiCl_4$	1.03	28a
$[Me_3P(CO)_3(NO)W]^+$	0.93	29
$SnCl_4$	0.87	28a
$CpMo(CO)_3^+$	0.70	29
Et_3Al	0.63	28a
$CpFe(CO)_2^+$	0.54	29

[a] Based upon the relative downfield shift of H_3 upon coordination of crotonaldehyde.

dienophile such as methyl acrylate is used, considerable polymerization of butadiene takes place, forming a viscous oil, which is insoluble in nitromethane-d_3. The scope of the catalytic properties of these Lewis acids and the mechanistic implications will be the subject of further investigation.

η^1 versus η^2 Binding. The $[HC(py)_3M(NO)_2]^{2+}$ Lewis acids have been shown to be strong and relatively hard acids. No η^2 binding was directly observed with aldehydes, ketones, or esters. In the case of aldehydes, separate signals for free and bound aldehyde were observed and the NMR chemical shifts were the primary evidence for η^1 binding. Since no separate resonance for an η^2-bound aldehyde was observed, it is possible that such a species was present in low concentration and exchanging rapidly with either the free or η^1-bound aldehyde. Although at lower temperatures a separate resonance for an η^2-bound species was never observed, in some instances (low free aldehyde concentration) broadening of the "free" aldehyde resonance was observed, even at room temperature. When the temperature was from -40 °C to +40 °C for benzaldehyde with $[HC(py)_3W(NO)_2]^{2+}$, the "free" resonance progressed from a fairly narrow line to a broad resonance (7 Hz) at 10 °C and back to a narrower line, yet it did not show an appreciable shift (~0.02 ppm).[31] This result is consistent with exchange between a very low concentration species and free aldehyde. We attribute this behavior to relatively facile exchange between free aldehyde and a weakly bound η^2-aldehyde species in very low concentration (<1%). Since no broadening was observed in the η^1-aldehyde resonance, the η^1-aldehyde cannot be interconverting with the η^2 complex rapidly. Therefore, we conclude that the rapid rearrangements between syn and anti isomers in an η^1 complex cannot involve an η^2 intermediate in these complexes. In this context, we favor a transition state in which the metal remains in the CHO plane during the "migration from one oxygen lone pair to the other". By analogy to theoretical analyses for main-group Lewis acid migrations,[32] this path appears more favorable than one involving out-of-plane structures. The relatively low barrier to this migration suggests that one consider a process involving continual rehybridization of the lone-pair orbital throughout this motion to maintain a strong σ bond to the metal. Hence, the transition state would involve an sp donor orbital with the lone pair in a p orbital, rather than both pairs utilizing the sp^2 hybrids of the ground states.

Similar evidence for a small fraction of η^2-ester exchanging with free ester, but not with η^1-ester, can be observed in the spectra of the methyl acetate adduct (Figure 5).[33] This suggests that the path for syn-anti migration of the metal in ester complexes is similar to that described for the aldehyde adducts.

Acknowledgment is made to the donors of the Petroleum Research Fund, administered by the American Chemical Society, for support of this research. We also thank Drs. D. L. White, C. Blankenship, L. Maheu, and B. Whitmore for their contributions to the development of better procedures for the preparation of $HC(py)_3$.

(31) The amount of the shift varied with the relative concentration of free aldehyde. The broadening was usually clearly observable at high fields. At lower fields (<250 MHz) and higher relative concentrations ([aldehyde]: [complex] >2), sharp resonances were observed for the "free" aldehyde.
(32) LePage, T. J.; Wiberg, K. B. *J. Am. Chem. Soc.* **1988**, *110*, 6642.
(33) Ma, Y. Ph.D. Dissertation, Yale University, New Haven, CT, May 1989.

Reversible Two-Electron–One-Proton Systems in the Ring-Centered Oxidation of Metalloporphyrins Bearing Secondary Amide-Linked Superstructures

Asma El-Kasmi,[1a] Doris Lexa,[1a] Philippe Maillard,[1b] Michel Momenteau,[1b] and Jean-Michel Savéant*,[1a]

Contribution from the Laboratoire d'Electrochimie Moléculaire de l'Université de Paris 7, Unité Associée au CNRS 438, 2 Place Jussieu, 75251 Paris Cedex 05, France, and the Institut Curie, Section de Biologie Unité Inserm 219, 91405 Orsay, France. *Received August 6, 1990*

Abstract: Complexes of porphyrins derived from tetraphenylporphyrin by substitution of the ortho position of the phenyl rings by secondary amide groups in a basket-handle or picket configuration undergo a reversible two-electron oxidation whatever the nature of the central metallic ion, Cu^{2+}, Zn^{2+}, Ni^{2+}, Fe^{3+}, Co^{3+}, in solvents such as 1,2-dichloroethane, methylene chloride, and benzonitrile. The reaction mechanism is investigated by cyclic voltammetry (as a function of the scan rate and the addition of a base or an acid) and UV-vis-near-IR and Fourier transform IR thin-layer spectroelectrochemistry. The reaction product is an endogeneous isoporphyrin resulting from the formation of an oxazine ring formed upon condensation of a meso carbon of the porphyrin dication with the oxygen of the amide group. The same reaction occurs with tertiary amide substituents, but in the case of secondary amide the concomitant loss of the amide proton facilitates the formation of the isoporphyrin. It thus drives the uphill disproportionation of two cation radicals to the right-hand side to such an extent that the uptake of the two electrons takes place at nearly the same potential. The reduction of the internal isoporphyrin is also a two-electron reaction at low scan rates with both the secondary and tertiary amide substituted compounds. The two-electron character of the isoporphyrin reduction is the result of an autocatalytic process in which the porphyrin cation radical serves as redox catalyst.

Metalloporphyrins bearing superstructures attached to the porphyrin ligand by means of secondary amido groups have been extensively employed to mimic the role of the proteinic environment of the prosthetic group of hemoglobin and myoglobin in

0002-7863/91/1513-1586$02.50/0

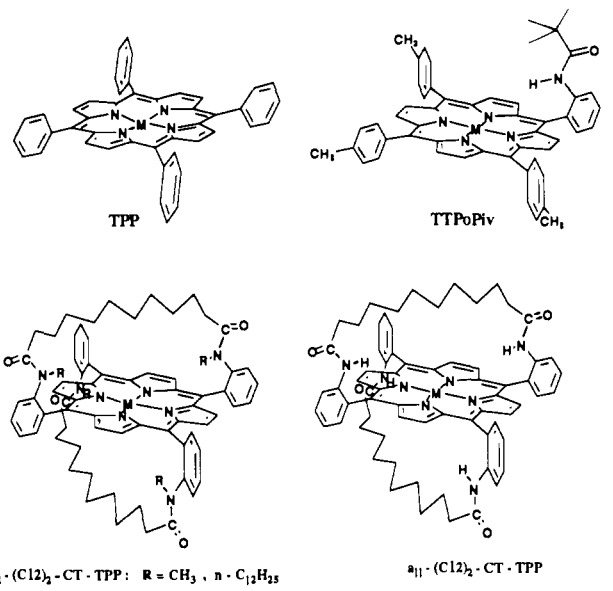

Figure 1. Porphyrin structures and conventional designations.

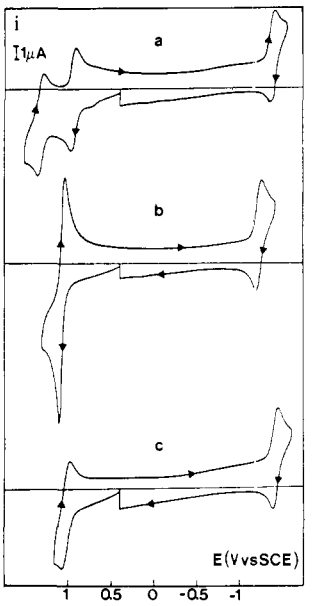

Figure 2. Cyclic voltammetry of TPPCu (a), a_H-(C12)$_2$-CT-TPPCu (b), and a_{CH_3}-(C12)$_2$-CT-TPPCu (c) in 1,2-dichloroethane + 0.1 M NBu_4PF_6 at a glassy carbon electrode. Porphyrin concentration: 0.5 mM. Scan rate: 0.1 V s^{-1}. Temperature: 17 °C. The potentials are referred to the aqueous saturated calomel electrode. Cathodic currents are represented as positive.

dioxygen binding and dioxygen vs carbon monoxide discrimination.[2] On the other hand, the secondary amide groups in such systems, when present in the close vicinity of the porphyrin ring, have been shown to exert a strong influence on the redox and ligand binding thermodynamics of the central metal in the case of iron(II), -(I) or -(0).[3]

Another striking effect of the secondary amide groups observed with copper, zinc, and magnesium basket-handle tetraphenyl porphyrins concerns their oxidation into the corresponding cation radicals and dications.[4a] In nonnucleophilic or poorly nucleophilic solvents such as methylene chloride or benzonitrile, simple porphyrins, such as TPP,[5] exhibit two well-separated, reversible, one-electron cyclic voltammetric oxidation waves corresponding to the successive formation of the cation radical and the dication. These species are sufficiently stable to be fully rereduced at scan rates as low as 0.1 V s^{-1}. In contrast, secondary amide linked basket-handle and picket-fence porphyrins exhibit, at low scan rates, a reversible two-electron oxidation pattern.[4] That this behavior is related to the presence of the NHCO groups rather than to the surrounding of the porphyrin rings by carbon chains is shown by the fact that the presence of chains of similar structure but attached by ether groups does not induce such a dramatic change of the oxidation pattern.[4a] ECE-type mechanisms,[6] in which a reversible chemical transformation, C, of the cation radical would make the second electron transfer (E) step easier than the first (E), have been invoked to rationalize these findings.[4a] However, the nature of this chemical step has not been established.[4d]

The purpose of the work reported here was to unravel the mechanism by which the reversible two-electron oxidation occurs. In this purpose, our strategy was the following. Related superstructured porphyrins in which the secondary amides are replaced by tertiary amides were prepared, and the study of their cyclic voltammetry led to the conclusion that NHCO protons are involved in the reaction. A one-NHCO-picket porphyrin instead of the usual four-NHCO porphyrin was prepared, and its oxidation patterns were investigated. The reversible two-electron behavior still observed showed that the participation of only one amide

(1) (a) Université de Paris 7. (b) Institut Curie.

(2) (a) For reviews on the purposes and syntheses of superstructured porphyrins see refs 2c–j. (b) These porphyrins belong to two main groups: those derived from the etioporphyrin ring in which the chains are attached to ethyl substituents borne by the pyrrole rings[2k] and those derived from the tetraphenylporphyrin structure where the chains are attached to the phenyl rings by means of *o*-NHCO substituents giving rise to "picket fence",[2c] "basket-handle",[2j,l–o] "pocket-picket",[2p] "picknic basket",[2g,r] and "jelly-fish"[2s,t] structures. (c) Collman, J. P. *Acc. Chem. Res.* **1977**, *10*, 265. (d) Jones, R. D.; Summerville, D. A.; Basolo, F. *Chem. Rev.* **1979**, *79*, 139. (e) Smith, P. D.; James, B. R.; Dolphin, D. H. *Coord. Chem. Rev.* **1981**, *39*, 31. (f) Traylor, T. G. *Acc. Chem. Res.* **1981**, *14*, 102. (g) Bogatskii, A. V.; Zhilina, Z. I. *Russ. Chem. Rev.* **1982**, *51*, 592. (h) Collman, J. P.; Halpert, T. R.; Suslick, K. S. *Metal Ion Activation of Dioxygen*; Spiro, T. G., Ed.; Wiley: New York, 1980; pp 1–72. (i) Baldwin, J. E.; Perlmutter, P. Bridged, Capped and Fenced Porphyrins. *Top. Curr. Chem.* **1984**, *121*, 181. (j) Dolphin, D. H. *Structure and Bonding*; Springer-Verlag: Berlin, 1987; pp 116–203. (k) Traylor, T. G.; Tsuschiva, S.; Campbell, D.; Mitchell, M.; Stynes, D.; Koga, N. *J. Am. Chem. Soc.* **1985**, *107*, 604. (l) Momenteau, M.; Scheidt, W. R.; Eigenhot, C. W.; Reed, C. A. *J. Am. Chem. Soc.* **1988**, *110*, 1207. (m) Maillard, P.; Schaeffer, C.; Tetreau, C.; Lavalette, D.; Lhoste, J.-M.; Momenteau, M. *J. Chem. Soc., Perkins Trans. 2* **1989**, 1437. (n) Desbois, A.; Momenteau, M.; Lutz, M. *Inorg. Chem.* **1989**, *28*, 825. (o) Momenteau, M. Actualité Chimique. **1989**, *4*, 95. (p) Boitrel, B.; Lecas, A.; Rose, E. *Tetrahedron Lett.* **1988**, *29*, 5653. (q) Collman, J. P.; Brauman, J. I.; Fitzgerald, J. P.; Sparapany, J. W.; Ibers, J. A. *J. Am. Chem. Soc.* **1988**, *110*, 3486. (r) Collman, J. P.; Brauman, J. I.; Fitzgerald, J. P.; Hampton, P. D.; Naruta, Y.; Michida, T. *Bull. Chem. Soc. Jpn.* **1988**, *61*, 47. (s) Uemori, Y.; Miyakawa, H.; Kyuno, E. *Inorg. Chem.* **1988**, *27*, 377. (t) Uemori, Y.; Kyuno, E. *Inorg. Chem.* **1989**, *28*, 1691.

(3) (a) Lexa, D.; Momenteau, M.; Rentien, P.; Rytz, G.; Savéant, J-M.; Xu, F. *J. Am. Chem. Soc.* **1984**, *106*, 4755. (b) Lexa, D.; Momenteau, M.; Savéant, J-M.; Xu, F. *Inorg. Chem.* **1985**, *24*, 122. (c) Croisy, A.; Lexa, D.; Momenteau, M.; Savéant, J-M. *Organometallics* **1985**, *4*, 1574. (d) Lexa, D.; Savéant, J-M.; Wang, D. L. *Organometallics* **1986**, *5*, 1428. (e) Gueutin, C.; Lexa, D.; Momenteau, M.; Savéant, J-M.; Xu, F. *Inorg. Chem.* **1986**, *25*, 4294. (f) Lexa, D.; Momenteau, M.; Mispelter, J.; Savéant, J-M. *Inorg. Chem.* **1989**, *28*, 30. (g) Lexa, D.; Savéant, J-M. In *Redox Chemistry and Interfacial Behavior of Biological Molecules*; Dryhurst, G., Niki, K., Eds.; Plenum Press: New York, 1988; pp 1–23. (h) Lexa, D.; Momenteau, M.; Savéant, J-M.; Xu, F. *Inorg. Chem.* **1986**, *25*, 4857. (i) Lexa, D.; Maillard, P.; Momenteau, M.; Savéant, J-M. *J. Phys. Chem.* **1987**, *91*, 1951. (j) Gueutin, C.; Lexa, D.; Savéant, J-M.; Wang, D. L. *Organometallics* **1989**, *8*, 1613. (k) Hammouche, M.; Lexa, D.; Savéant, J-M. *J. Electroanal. Chem. Interfacial Electrochem.* **1988**, *249*, 347. (l) Lexa, D.; Momenteau, M.; Savéant, J-M.; Xu, F. *J. Am. Chem. Soc.* **1986**, *108*, 6937. (m) Lexa, D.; Savéant, J-M.; Su, K. B.; Wang, D. L. *J. Am. Chem. Soc.* **1988**, *110*, 7617.

(4) (a) Lexa, D.; Maillard, P.; Momenteau, M.; Savéant, J-M. *J. Am. Chem. Soc.* **1984**, *106*, 6321. (b) A similar behavior has also been recently observed in the oxidation of a nickel picket fence porphyrin.[4c] (c) Kadish, K. M.; Sazou, D.; Maiya, G. B.; Han, B. C.; Liu, Y. M.; Saoiabi, A.; Ferhat, M.; Guilard, R. *Inorg. Chem.* **1989**, *28*, 2542. (d) A tentative hypothesis was a flipping of the NHCO group giving rise to a mechanism similar to those involving conformational changes in organic molecules.[4e] (e) Evans, D. H.; O'Connel, K. M. *Electroanalytical Chemistry*; Bard, A. J., Ed.; Dekker: New York, 1986; pp 113–207.

(5) See Figure 1 for the definition of the abbreviations designating the porphyrins employed in the paper.

(6) Andrieux, C. P.; Savéant, J-M. Electrochemical Reactions. In *Investigation of Rates and Mechanisms*; Bernasconi, C. F., Ed.; Wiley: New York; 1986.

Table I. Cyclic Voltammetric Characteristics of the Oxidation of Simple and Superstructured Porphyrins in 1,2-Dichloroethane[a]

	first wave				second wave			
porphyrin[b]	E^{0}[c]	n	reversibility	ΔE_p[d]	E^{0}[c]	n	reversibility	ΔE_p[d]
copper(II) complexes								
TPP	0.975	1	rev	63	1.355	1	rev	70
a_H-$(C_{12})_2$-CT-TPP	1.100	2	rev	60				
a_{CH_3}-$(C_{12})_2$-CT-TPP	1.060	1	rev	100	1.345[e]	1	irrev	
$a_n C_{12}H_{25}$-$(C_{12})_2$-CT-TPP	1.080	1	rev	88	1.400[e]	1	irrev	
TTPoPiv	1.05	2	rev	70				
zinc(II) complexes								
TPP	0.800	1	rev	60	1.120	1	rev	70
a_H-$(C_{12})_2$-CT-TPP	0.920	2	rev	75				
a_{CH_3}-$(C_{12})_2$-CT-TPP	0.930	1	rev	100	1.160[e]	1	irrev	
nickel(II) complexes								
TPP	0.985	1	rev	85	1.275	1	rev	120
a_H-$(C_{12})_2$-CT-TPP	1.165	2	rev	93				
TTPoPiv	1.080	2	rev	160				
iron(III) complexes								
TPP	1.085	1	rev	64	1.480	1	rev	77
a_H-$(C_{12})_2$-CT-TPP	1.110	2	rev	156				
TTPoPiv	1.095	2	rev	146				
cobalt(III) complexes								
TPP	1.125	1	rev	62	1.410	1	rev	76
a_H-$(C_{12})_2$-CT-TPP	1.090	2	rev	100				

[a] +0.1 M NBu_4PF_6. Scan rate: 0.1 V s^{-1}. Temperature: 17 °C. [b] See figure 1 for definition of the conventional designations. [c] Standard potential in V vs SCE unless otherwise stated. [d] Potential difference (in mV) between the anodic and cathodic peaks. [e] Anodic peak potential at 0.1 V s^{-1} in V vs SCE.

proton is required. The product of the $-2\ e^- - H^+$ oxidation was identified as being an internal isoporphyrin in which the oxygen atom of the carbonyl group binds to the vicinal meso carbon of the porphyrin ring while the amide proton is expelled. The reaction mechanism was further analyzed by investigating the effect of the addition of a base and an acid on the cyclic voltammetric patterns as well as the effect of scan rate variations.

On the whole, a new two-electron–one-proton reversible redox system, unprecedented in porphyrin chemistry, was thus discovered. It provides an example of how neighboring secondary amide groups may intimately participate in the oxidation chemistry of porphyrins through the formation of isoporphyrins.[7]

Results and Discussion

The various porphyrin structures employed in the present study are shown in Figure 1 together with their conventional designations.

Figure 2 shows the slow-scan (0.1 V s^{-1}) cyclic voltammogram of the simple copper(II) tetraphenylporphyrin and those of two copper basket-handle tetraphenylporphyrin in which the two 12-carbon chains are linked to the ortho position of the phenyl rings by secondary and tertiary amide groups, respectively. The potential was scanned so as to encompass both the oxidation and reduction waves. The reversible reduction wave observed in all three cases has the same height and can thus serve as a standard for a one-electron reversible process. Two clearly separated reversible one-electron oxidation waves are observed with TPPCu. The secondary amide linked basket-handle porphyrin exhibits a single two-electron reversible oxidation wave. Quite similar results were obtained with other metals, namely, zinc, nickel, iron, and cobalt, complexed by the same a_H-$(C12)_2$-CT-TPP ligand (Table I). In the case of Cu, Zn, and Ni porphyrins the reversible two-electron oxidation wave is obtained upon oxidation of the metal(II) porphyrins, whereas with Fe and Co it is observed upon oxidation of the metal(III) porphyrin. The tertiary amide linked basket-handle copper(II) porphyrins in which the amide hydrogen has been replaced by a methyl or in which a *n*-dodecyl group

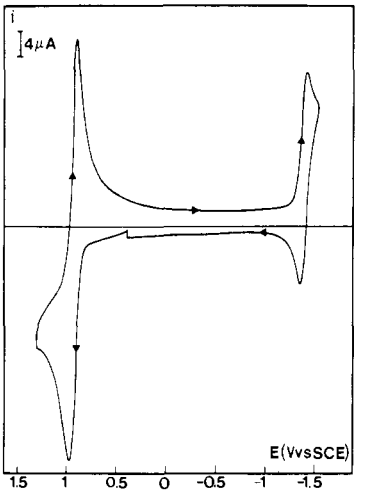

Figure 3. Cyclic voltammetry of TTPoPivCu (5 mM) in 1,2-dichloroethane + 0.1 M NBu_4BF_4 at a glassy carbon electrode. Scan rate: 0.1 V s^{-1}. Temperature: 17 °C. The potentials are referred to the saturated calomel electrode. Cathodic currents are represented as positive.

exhibits a one-electron reversible oxidation wave[8] (see Figure 2b and Table I). We infer from this observation that the protons of the secondary amide groups partake in the mechanism responsible for the observation of a reversible two-electron oxidation reaction.

How many secondary amide protons are required to obtain the two-electron reversible oxidation pattern? The answer is provided by examination of the cyclic voltammetry of the copper(II) porphyrin designated TTPoPiv (Figure 1) in which a single pivalamido picket is grafted in the ortho position of one phenyl ring. As seen in Figure 3, a two-electron reversible oxidation wave is again observed, pointing to the conclusion that only one secondary amide proton is required in the reaction. The overall reaction is thus a two-electron–one-proton reversible process:

$$MP \rightleftharpoons 2e^- + H^+ + MP'$$

The same cyclic voltammetric behavior was found with the

(7) (a) Exogenous isoporphyrins are obtained upon reaction of porphyrin dications with a variety of nucleophiles.[7b] They have also been detected as side products in the oxidation of models compounds of cytochrome P-450[7c,d] and in reactions of peroxidases.[7e] (b) Dolphin, D.; Halko, D. J.; Johnson, E. C.; Rousseau, K. *Porphyrin Chemistry Advances*; Long, F. R., Ed.; Ann Arbor Science: Ann Arbor, MI 1979; p 120. (c) Guzinski, J. A.; Felton, R. A. *J. Chem. Soc., Chem. Commun.* **1973**, 715. (d) Gold, A.; Ivey, W.; Toney, G. E.; Sangaiah, R. *Inorg. Chem.* **1984**, *23*, 2932. (e) Ator, M. A.; David, S. K.; Ortiz de Montellano, P. R. *J. Biol. Chem.* **1989**, *264*, 9250.

(8) A second oxidation wave (not represented in Figure 2) is observed at more positive potentials. It is irreversible in both cases unlike the case of TPPCu. We will come back to this point later on.

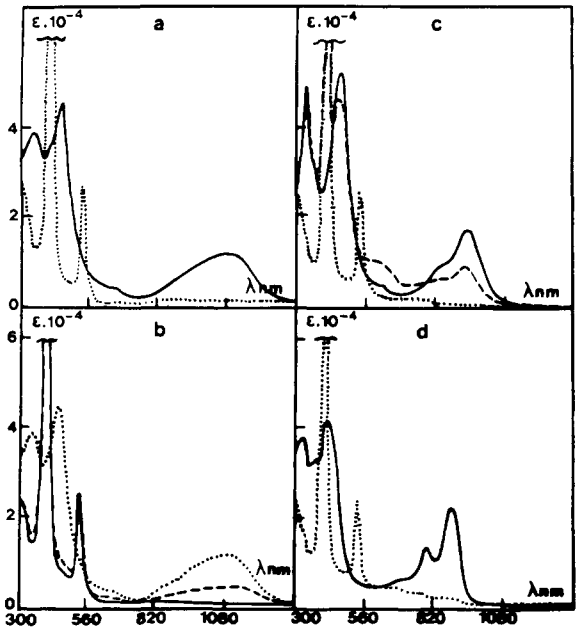

Figure 4. Thin-layer UV–vis–near-IR spectroelectrochemistry (in 1,2-dichloroethane + 0.1 M NBu_4PF_6 at a platinum grid electrode) of (a) a_H-$(C_{12})_2$-CT-TPPCu with no applied potential (···), after 30 min of electrolysis at 1.35 V vs SCE (—); (b) a_H-$(C12)_2$-CT-TPPCu after 30 min of electrolysis at 1.35 V vs SCE (···), after 15 min of rereduction at 0.80 V vs SCE (---), after 15 min more of rereduction at 0.8 V vs SCE (—); (c) TPPoPivCu with no applied potential (···), after 15 min of electrolysis at 1.25 V vs SCE (---), after 15 min more of electrolysis at 1.25 V vs SCE (—); (d) TPPCu + MeOH (6 mM) with no applied potential (···), after 30 min of electrolysis at 1.05 V vs SCE (—). Porphyrin concentration: 0.2 mM. Temperature: 21 °C.

TTPoPivNi(II) and TTPoPivFe(III)Cl porphyrins.

What is the nature of the species designated MP′? was the next question to be answered. A first indication was provided by the UV–vis–near-IR spectrum obtained by electrolysis in a thin-layer spectroelectrochemical cell. Figure 4 shows the spectra thus obtained with the a_H-$(C12)_2$-CT-TPPCu and TTPoPivCu porphyrins as well as those obtained with TPPCu upon oxidation in the same solvent after addition of methanol. As shown by previous studies, this spectrum (Figure 4d) characterizes the formation of the corresponding isoporphyrin:[7b]

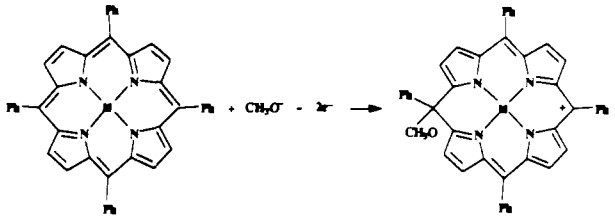

It is seen that the spectra obtained for the a_H-$(C12)_2$-CT-TPPCu (Figure 4a,b) and TTPoPivCu (Figure 4c) are clearly of the isoporphyrin type and not of the dication type. It is remarkable that with these two porphyrins the spectrum of the starting complex could be regenerated upon reduction of the MP′ complex at a potential slightly negative to the two-electron reversible wave (Figure 4b). It was also observed that a small amount of the cation radical[9] appears transitorily during the oxidation electrolysis (see, for example, the band at 600 nm in Figure 4c) as well as during the rereduction electrolysis.

Quite similar isoporphyrin UV–vis–near-IR spectra were obtained with all the other secondary amide substituted porphyrins listed in Table I.

This set of observations suggests that the oxidation of the porphyrins containing at least one secondary amide group at the ortho position of a phenyl ring leads to the formation of an internal isoporphyrin according to

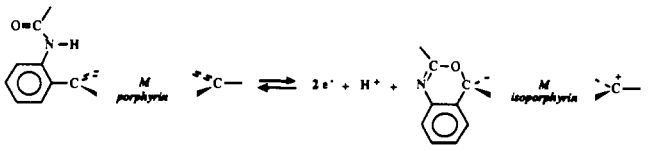

This was confirmed by thin-layer Fourier transform infrared spectroelectrochemistry. The TTPoPivCu porphyrin was selected for this study rather than a basket-handle porphyrin because the transformation involving one secondary amide group is expected to appear more clearly in the absence of other, unchanged secondary amide groups. As seen in Figure 5, the N—H (3428 cm^{-1})[10a] (Figure 5a) and C=O (1682 cm^{-1})[10a] (Figure 5b) bands in the starting complex decrease and disappear upon oxidation at 1.3 V vs SCE while new bands develop at 1610, 1184, and 1080 cm^{-1} (Figure 5c). The band at 1610 cm^{-1} can be assigned to a C=N group in a six-atom heterocycle containing an oxygen atom,[10b] whereas the 1184- and 1080-cm^{-1} bands are assignable to the asymmetrical and symmetrical vibrations of the C—O—C group, respectively.[10a,c] Upon rereduction at 0.7 V vs SCE, these new bands disappear and the bands of the starting complex reappear, confirming the reversibility of the $2e^- + H^+$ redox process.

The same characteristic and evolution of the FTIR spectra were found with the TTPoPivNi(II) and TTPoPivFe(III)Cl porphyrins.

The anodic-to-cathodic peak separation in cyclic voltammetry (Table I) is close to the theoretical value (60 mV) for the first reversible oxidation wave of the TPP complexes, indicating that the electron transfer is rapid.[6,11] For the reversible two-electron wave obtained with TTPoPivCu and the a_H-$(C12)_2$-CT-TPP complexes, the peak separation is of the order of 60–70 mV. Such a magnitude for the peak separation of a reversible two-electron wave indicates that the product of the first electron transfer is

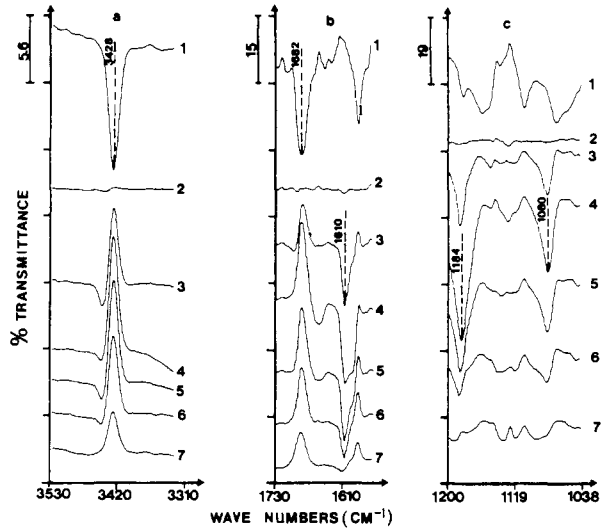

Figure 5. Thin-layer FTIR spectroelectrochemistry in 1,2-dichloroethane + 0.1 M NBu_4PF_6 at a platinum grid electrode of TTPoPivCu (3 mM). Curve 1 is the initial spectrum of the porphyrin; all the other curves show difference spectra obtained by addition of curve 1. Thus (2), obtained with no applied potential, represents the base line. (3) After 12 min of oxidation at 1.3 V vs SCE. (4) After 22 min of oxidation at 1.3 V vs SCE. (5) After 10 min of rereduction at 0.7 V vs SCE. (6) After 20 min of rereduction at 0.7 V vs SCE. (7) After 120 min of rereduction at 0.7 V vs SCE. Temperature: 21 °C. (a) N-H band; (b) C=O and C=N bands; (c) C—O—C bands.

(9) Dolphin, D.; Muljiani, Z.; Rousseau, K.; Borg, D. C.; Fajer, J.; Felton, R. H. *Ann. N. Y. Acad. Sci.* **1973**, *206*, 177.

(10) (a) Bellamy, L. J. *The Infrared Spectra of Complex Molecules*; Chapman and Hall: London, 1975. (b) Katritzky, A. R. *Physical Methods in Heterocyclic Chemistry*; Academic Press: New York, 1963; Vol. II, pp 248–249. (c) Wojtkowiak, B.; Chabanel, M. *Spectrochimie Moléculaire*; Technique et Documentation: Paris, 1977.

(11) Bard, A. J.; Faulkner, L. R. *Electrochemical Methods*; Wiley: New York, 1980.

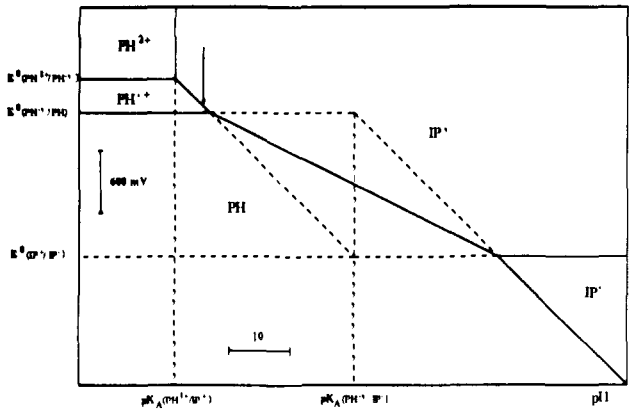

Figure 6. Schematic E^0 - pH diagram involving the various species shown in Scheme I.

Scheme I

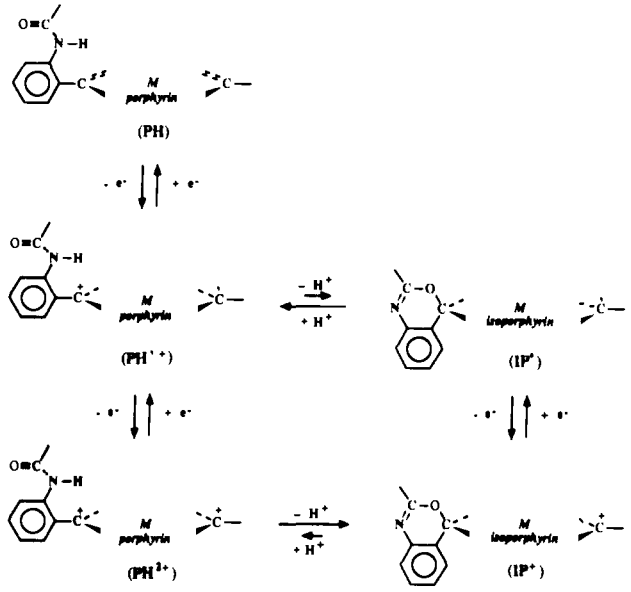

chemically stable. An anodic-to-cathodic peak separation of 60 mV is expected for a disproportionation

$$2PH^{\bullet+} \rightleftarrows PH + IP^+ + H^+$$

equilibrium constant of 0.25.[12] That the electron-transfer stability of the cation radical is of the same order of magnitude is confirmed by the fact that the spectrum of the cation radical is observed transiently upon oxidation and rereduction of the complex at potentials positive and negative to the standard potential of the two-electron reversible wave, respectively.

Two consequences ensue. One is that the chemical reaction responsible for the two-electron–one-proton reversible process does not affect the one-electron oxidation intermediate, i.e., the cation radical but rather the dication. The formation of the final internal isoporphyrin complex should then result from the deprotonation of the dication. The second consequence is that the thermodynamic characteristics of the system are of the type shown schematically in the E^0–pH diagram in Figure 6, where the various intervening complexes are those represented in Scheme I. In the neat solvent, the slow-scan cyclic voltammetric two-electron reversible wave (Figure 2b) corresponds to the thermodynamic conditions depicted in Figure 6 by the vertical arrow.

Turning back to the case of tertiary amide substituents, the question arises whether they can form isoporphyrins upon oxidation even though they do not give rise to a reversible two-electron–one-proton system as the porphyrins bearing secondary amides do. Figure 7 shows the results of a more detailed cyclic voltammetric analysis of the oxidation and rereduction patterns of the a_{CH_3}-$(C12)_2$-CT-TPPCu complex.

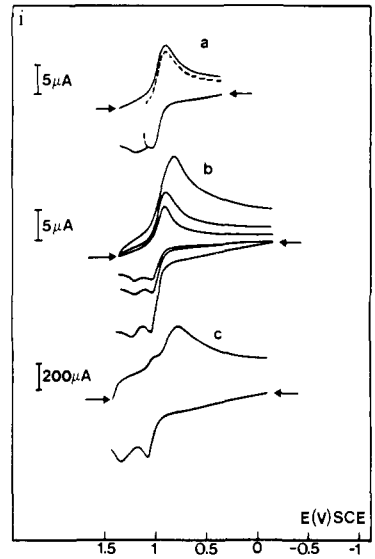

Figure 7. Cyclic voltammetry of a_{CH_3}-$(C12)_2$-CT-TPPCu (0.8 mM) in 1,2-dichloroethane + 0.1 M NBu_4PF_6 as a function of the scan rate. Temperature: 17 °C. Cathodic currents are represented as positive. The anodic waves are recorded, starting, as represented by the arrows, at a potential negative to the wave. The cathodic rereduction waves are recorded, as represented by the arrows, from the same porphyrin solution after setting the potential for ca. 1 min behind the anodic waves. Scan rate: 0.1 (a), 0.05, 0.1, 0.3 (b), 5 (c) V s^{-1}. (a) The dashed line represents the first oxidation wave.

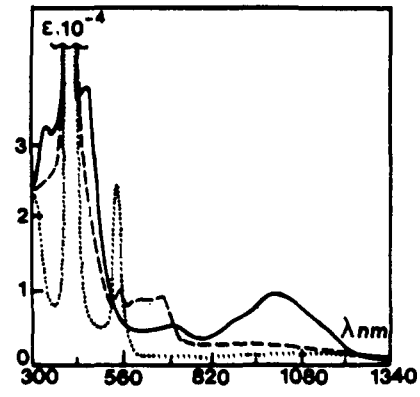

Figure 8. Thin-layer UV-vis-near-IR spectroelectrochemistry of a_{CH_3}-$(C12)_2$-CT-TPPCu (0.2 mM) in 1,2-dichloroethane + 0.1 M NBu_4PF_6 Temperature: 21 °C. With no potential applied (···); after electrolysis at 1.3 V vs SCE (---); after electrolysis at 1.4 V vs SCE (—).

The first one-electron reversible oxidation wave, already shown in Figure 2c, is followed by a somewhat smaller irreversible wave. Upon scan reversal, under conditions where the two-electron oxidation product has replaced the starting compound in the diffusion layer (see caption of Figure 7), a two-electron rereduction wave is observed at low scan rate. Raising the scan rate makes a second reduction wave appear at the expense of the first (Figure 7c), which eventually disappears.[14]

The oxidation products at the first and second wave were identified by thin-layer UV-vis-near-IR spectroelectrochemistry (Figure 8). The cation radical is obtained at the first wave and is stable enough to be rereduced into the starting compound. An

(12) (a) Ammar, F.; Savéant, J-M. *J. Electroanal. Chem.* **1973**, *47*, 115. (b) Ammar, F.; Savéant, J-M. *J. Electroanal. Chem.* **1973**, *47*, 215.

(13) The standard potentials were roughly estimated from the cyclic voltammetric peak potentials obtained upon addition of acid (see Figure 10).

(14) (a) This behavior is similar to that reported for an isoporphyrin generated from the reaction of the dication with nitrate ion as exogenous nucleophile or that exhibited by an isoporphyrin produced from a water-soluble porphyrin in aqueous media at pH 4.[14c] (b) Hinman, A. S.; Pavelich, B. D.; Kondo, A. E.; Pons, S. *J. Electroanal. Chem.* **1987**, *234*, 145. (c) Su, Y. O.; Kim, D.; Spiro, T. G. *J. Electroanal. Chem.* **1988**, *246*, 363.

Scheme II

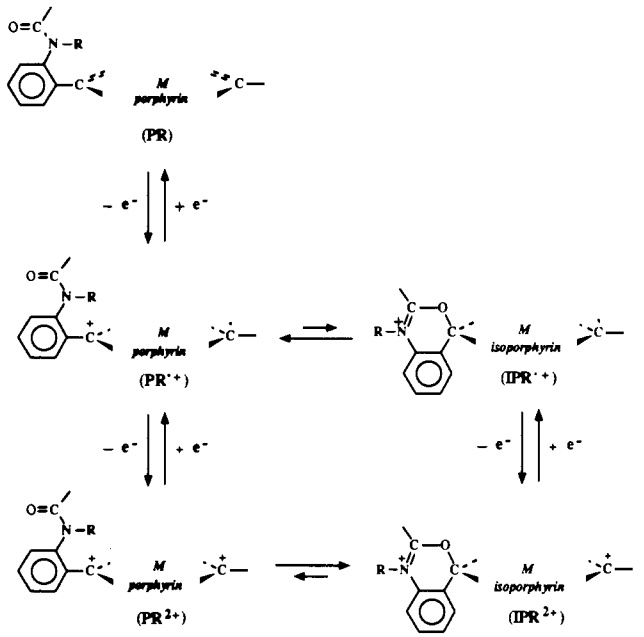

isoporphyrin spectrum is obtained at the second wave. The isoporphyrin can be entirely rereduced into the starting complex at a potential slightly negative to the two-electron rereduction wave observed in slow-scan cyclic voltammetry. The same features are observed with the a_{CH_3}-$(C12)_2$-CT-TPPZn porphyrin.

These observations suggest the involvement of the following species in the reaction mechanism (Scheme II). The irreversibility of the second oxidation wave is caused by the instability of the dication, PR^{2+}, which is converted into the isoporphyrin, IPR^{2+}, by formation of an oxazine ring resulting from the coupling of the amide oxygen with the porphyrin meso carbon. The reduction of the isoporphyrin dication, IPR^{2+}, observed at high scan rates, involves the direct reduction of this compound at the electrode surface, yielding the $IPR^{\bullet+}$ cation radical as an intermediate. This is immediately converted into the $PR^{\bullet+}$ cation radical by ring opening. The irreversibility of the conversion of $IPR^{\bullet+}$ into $PR^{\bullet+}$ is attested by the observation that $PR^{\bullet+}$ is stable within the time scale of slow-scan cyclic voltammetry and even within that of spectroelectrochemistry. The conversion of $IPR^{\bullet+}$ into $PR^{\bullet+}$ is the start of an ECE mechanism[6] since $PR^{\bullet+}$ is easier to reduce than IPR^{2+}. The second electron transfer may take place at the electrode surface (ECE) but also in solution by means of an electron transfer from $IPR^{\bullet+}$ to $PR^{\bullet+}$ (disproportionation):

$$IPR^{\bullet+} + PR^{\bullet+} \rightarrow IPR^{2+} + PR$$

This is a downhill process since the $IPR^{2+}/IPR^{\bullet+}$ couple is largely negative to the $PR^{\bullet+}/PR$ couple.

At lower scan rates (Figure 7a), a two-electron wave is observed in the potential region of the $PR/PR^{\bullet+}$ couple, i.e., much positive to the direct reduction of IPR^{2+}. This wave is the result of the following mechanism. The dication is mostly present at equilibrium under its isoporphyrin form, IPR^{2+}. However, the small amount present under the porphyrin form, PR^{2+}, can be reduced in the potential region of the second oxidation wave, i.e., at a very positive potential, along a CE mechanism:[6]

$$IPR^{2+} \rightleftharpoons PR^{2+} \text{ (C)} \qquad PR^{2+} + e^- \rightleftharpoons PR^{\bullet+} \text{ (E)}$$

Equilibrium being much in favor of IPR^{2+}, the corresponding wave is hardly detectable on the cyclic voltammograms. As the potential approaches the potential region of the $PR^{\bullet+}/PR$ couple, a second wave develops corresponding the reduction of $PR^{\bullet+}$:

$$PR^{\bullet+} + e^- \rightleftharpoons PR$$

If this were the only reaction taking place, the wave should be of the same height as the $PR^{2+}/PR^{\bullet+}$ CE wave, i.e., undetectably small. However, an autocatalysis process is then triggered by the

Scheme III

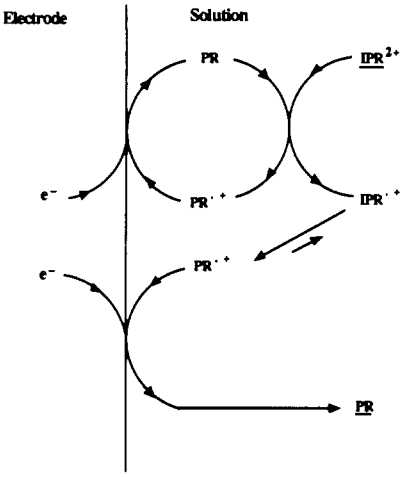

Scheme IV

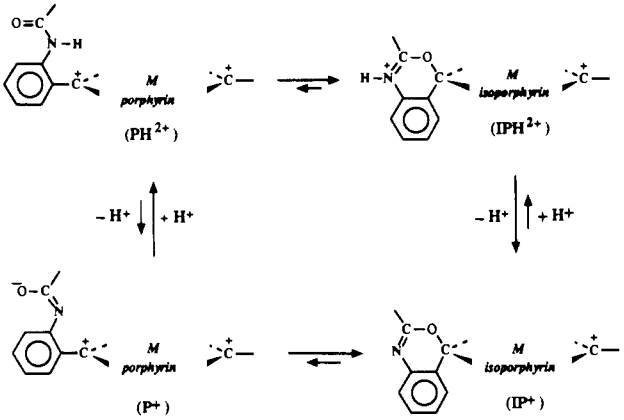

production of a small amount of PR (Scheme III). In this process, the $PR^{\bullet+}/PR$ couple works as a redox catalyst[6] for the reduction of IPR^{2+} (which requires a more negative potential to occur directly at the electrode surface):

$$PR + IPR^{2+} \rightleftharpoons PR^{\bullet+} + IPR^{\bullet+}$$

The only difference with usual redox catalysis[6] is that the catalyst, instead of being independent from the substrate to be reduced as it is in usual application, is presently the product of an initial reduction of the substrate (IPR^{2+}). The above chain-carrying electron-transfer reaction is an uphill process with an equilibrium constant of about 10^{-5}. The follow-up opening of the isoporphyrin oxazine ring is nevertheless sufficiently irreversible and fast, at the level of cation radicals, to efficiently drive the reaction toward the right-hand side. The overall rate constant is, however, not very large as attested by the fact that this wave starts to decrease and to become smaller than the two-electron height as the scan rate is made larger than 5 V s^{-1} and is then progressively replaced by the IPR^{2+}, more negative, direct reduction wave.

Having established the oxidation reduction mechanism of the tertiary amide substituted porphyrins, we can come back to the secondary amide case, which is somewhat more complicated since we must envisage the formation not only of the deprotonated isoporphyrin but also of a still protonated isoporphyrin by analogy to what has been elaborated in the alkyl-substituted case. The last reaction in Scheme I is thus an oversimplified representation of the actual mechanism along which the porphyrin dication is converted into the isoporphyrin cation. This in fact involves the square-scheme process shown in Scheme IV. Whether the conversion involves first ring closing followed by deprotonation, or vice versa, deprotonation followed by ring closing is not known. However, one should envisage that some still-protonated isoporphyrin, IPH^{2+}, is present, at equilibrium, together with a predominant amount of the deprotonated isoporphyrin, IP^+. The same questions arise for the deprotonation-ring closing/

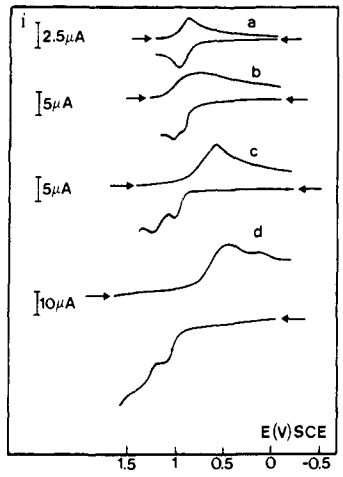

Figure 9. Cyclic voltammetry of TTPoPivCu (2 mM) in 1,2-dichloroethane + 0.2 M NBu_4PF_6. Temperature: 17 °C. Cathodic currents are represented as positive. The anodic and cathodic traces were obtained in the same way as described in the caption of Figure 7. Scan rates: 0.05 (a), 0.3 (b), 10 (c), 100 (d) V s^{-1}.

protonation–ring opening process at the cation radicals level. They are, however, of much less importance since the reaction goes irreversibly from $IP^{\bullet}$ to $PH^{\bullet+}$ as attested by the chemical stability of the latter compound observed in spectroelectrochemical experiments.

These considerations should be borne in mind in the analysis of the variations of the cyclic voltammograms when the scan rate is changed or when a base or an acid is added to the solution. Figure 9 shows the cyclic voltammetry of TTPoPivCu in the neat solvent as a function of scan rate. As this is raised, the two-electron oxidation wave splits into two waves that become eventually equal in height. Under the latter conditions, the first oxidation wave corresponds to the reversible oxidation of PH into $PH^{\bullet+}$ and the second to the irreversible oxidation of $PH^{\bullet+}$ into IP^+, the intermediate dication, PH^{2+}, being rapidly converted into IP^+ by one or the other routes depicted in Scheme IV. The reason a single two-electron oxidation wave is observed at low scan rates is that the cation radical, $PH^{\bullet+}$, disproportionates along the mechanism

$$2PH^{\bullet+} \rightleftharpoons PH + PH^{2+} \quad (1)$$

$$PH^{2+} \rightleftharpoons H^+ + IP^+ \quad (2)$$

The first of these two reactions is an uphill process, having an equilibrium constant of the order of 10^{-5}. It is, however, driven to the right-hand side by the follow-up irreversible conversion of the dication, PH^{2+}, into IP^+ by one or the other routes depicted in Scheme IV. The latter reaction is much more irreversible than the ring-closing reaction in the PR case, where no disproportionation enhancement of the first oxidation wave was observed (Figure 7). As a matter of fact, the negative charge resulting from the deprotonation of the secondary amide induces a much stronger driving force for ring closing.

In the rereduction process, three waves appear and vary in height at the expense of one another as the scan rate increases. The most negative, small wave that appears at the highest scan rates corresponds to the direct reduction of the deprotonated isoporphyrin, IP^+ (Figure 9d):

$$IP^+ + e^- \rightleftharpoons IP^{\bullet} \quad (3)$$

The latter species undergoes an irreversible protonation and ring opening (or vice versa), yielding the cation radical, $PH^{\bullet+}$:

$$IP^{\bullet} + H^+ \rightleftharpoons PH^{\bullet+} \quad (4)$$

Since $PH^{\bullet+}$ is much easier to reduce than IP^+, a second electron transfer occurs either at the electrode surface (ECE mechanism)

$$PH^{\bullet+} + e^- \rightleftharpoons PH \quad (5)$$

or in the solution (disproportionation mechanism)

$$PH^{\bullet+} + IP^{\bullet} \rightarrow PH + IP^+ \quad (6)$$

Scheme V

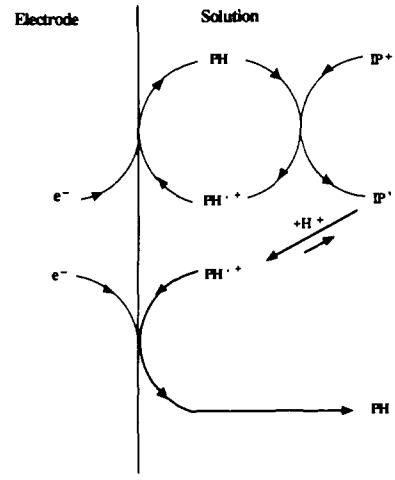

The second reduction wave that predominates at intermediate scan rates is located in a potential region close to that of the alkylated isoporphyrin IPR^{2+} described above. It corresponds to the reduction of the protonated isoporphyrin, IPH^{2+}, according to the following CE mechanism:

$$IP^+ + H^+ \rightleftharpoons IPH^{2+} \quad (7)$$

$$IPH^{2+} + e^- \rightleftharpoons IPH^{\bullet+} \quad (8)$$

$$IPH^{\bullet+} \rightleftharpoons PH^{\bullet+} \quad (9)$$

$$PH^{\bullet+} + e^- \rightleftharpoons PH \text{ and/or } PH^{\bullet+} + IPH^{\bullet+} \rightarrow PH + IPH^{2+} \quad (10)$$

Although the first of these reactions is an uphill process, the equilibrium constant is not too small and the protonation rate constant is large as attested by the fact that the appearance of the third wave at the expense of the second wave occurs only at rather high scan rates.

What is the mechanism responsible for the appearance of the first rereduction around the standard potential of the $PH^{\bullet+}/PH$ couple that predominates at low scan rates? The observations made with the tertiary amide compounds suggest that the same mechanism is also operating in the present case (Scheme III, where R would be replaced by H^+) involving as chain propagation step the electron transfer between PH and IPH^{2+}

$$PH + IPH^{2+} \rightleftharpoons PH^{\bullet+} + IPH^{\bullet+} \quad (11)$$

which has an equilibrium constant of the same order of magnitude (ca. 10^{-5}). In the present case too, the reaction is driven to the right-hand side by the irreversibility of the ring opening at the cation radical level:

$$IPH^{\bullet+} \rightleftharpoons PH^{\bullet+} \quad (12)$$

One should also a priori envisage the possibility of an autocatalysis process involving IP^+ as substrate rather than IPH^{2+} (Scheme V). However, the mechanism depicted in Scheme III (with H replacing R) certainly predominates over that depicted in Scheme V for the following reasons. The potential separation between the $PH/PH^{\bullet+}$ and $IP^+/IP^{\bullet}$ couples is at least 800 mV, meaning that the chain propagation step would have an equilibrium constant of 10^{-13} at maximum. Even if the follow-up deprotonation–ring opening (or vice versa) reaction would be so fast and irreversible as to make the $PH + IP^+$ reaction the rate-determining step, this would be too slow (10^{-3} M^{-1} s^{-1}, if the reverse reaction is at the diffusion limit) to produce any detectable effect on the cyclic voltammograms even at the lowest scan rates.

The oxidation reduction mechanism sketched above was confirmed by cyclic voltammetric experiments in which a base or an acid was added to the solution. As a base we selected 2,6-dimethylpyridine (2,6-lutidine) to sterically avoid the formation of

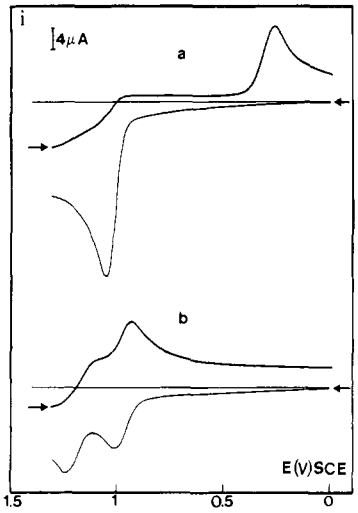

Figure 10. Slow scan (0.1 V s^{-1}) cyclic voltammetry of TTPoPivCu (2 mM) in 1,2-dichloroethane + 0.2 M NBu_4PF_6 in the presence of 20 mM 2,6-lutidine (a) and 0.8 M CF_3CO_2H (b). Temperature: 17 °C. Cathodic currents are represented as positive. The cathodic waves were obtained in the same way as described in the caption of Figure 7.

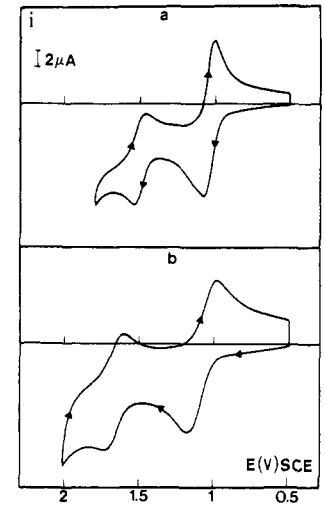

Figure 11. Cyclic voltammetry of TTPoPivCu (a) and TTPoPivNi (b) in 1,2-dichloroethane + 0.1 M NBu_4PF_6. Porphyrin concentration: 0.5 mM. Scan rate: 0.1 V s^{-1}. Temperature: 17 °C.

an exogenous isoporphyrin by reaction of the base with the porphyrin dication. That this is indeed the case was shown by the fact that the slow-scan cyclic voltammetry of TPPCu (two successive one-electron reversible waves) does not change upon addition of 2,6-lutidine to the solution. The effect of an addition of 2,6-lutidine on the slow-scan cyclic voltammetry of TTPoPivCu is shown in Figure 10a. A two-electron oxidation wave and a two-electron rereduction wave are observed, but they are now widely separated along the potential axis (ca. 800 mV), unlike the case of the neat solvent. The two-electron irreversible oxidation wave is located in the same potential region as the two-electron reversible oxidation wave observed in the neat solvent and thus corresponds to the same mechanism:

$$PH - e^- \rightleftarrows PH^{\bullet+},\ 2PH^{\bullet+} \rightleftarrows PH + PH^{2+},\ PH^{2+} \rightarrow H^+ + IP^+$$

The last reaction is expected to be faster than in the neat solvent. This is confirmed by the observation that the splitting in two waves requires much higher scan rates (ca. 50 V s^{-1} instead of ca. 0.5 V s^{-1}) to be observed. The single two-electron irreversible wave observed on the rereduction side is located at the same potential as the third rereduction wave (Figure 9d) observed in the neat solvent. It corresponds to the direct reduction of IP^+ along the ECE disproprotionation mechanism described earlier. The disappearance of the first and second rereduction waves even at low scan rates falls in line with the disappearance of the protonated isoporphyrin, IPH^{2+}, brought about by the introduction of 2,6-lutidine.

The introduction of an acid, viz., trifluoroacetic acid, brings the changes in the cyclic voltammograms shown in Figure 10b. The two-electron oxidation wave observed in the neat solvent is replaced by two successive one-electron waves as in the case of the tertiary amide compounds. This falls in line with the uphill disproportionation of the cation radicals, $PH^{\bullet+}$, being less driven to the right-hand side because the tendency for the dication to lose one proton and to undergo ring closing is decreased by the presence of the acid. On the reverse scan, two waves appear for the rereduction of the isoporphyrin which is now present mostly in its protonated form, IPH^{2+}. The first of these two waves, which appears at a potential positive to the $PH^{\bullet+}/PH$ couple, has the S-shape characteristic of a CE mechanism. It involves the reduction of the porphyrin dication, PH^{2+}, resulting from the predissociation of the isoporphyrin IPH^{2+}. It is now perfectly detectable in contrast to the observations made in the neat solvent, because the PH^{2+}/IPH^{2+} concentration ratio is larger than what it was in the neat solvent and larger than the PH^{2+}/IP^+ concentration. The second wave, located in the potential region of the $PH^{\bullet+}/PH$ couple, represents the autocatalyzed reduction of the IPH^{2+} isoporphyrin as described earlier. When the scan rate is raised, the two first waves decrease at the expense of a third wave representing the direct reduction of IPH^{2+} at the electrode surface (it is the same as the second reduction wave of the isoporphyrin in the neat solvent).

All the investigations described so far were carried out in 1,2-dichloroethane. We found very closely similar behaviors for all the porphyrins listed in Table I when using methylene chloride or benzonitrile as solvent.

We are thus led to conclude that, in both solvents, all the secondary amide substituted porphyrins listed in Table I undergo a reversible two-electron oxidation leading to the same internal isoporphyrin complex along the same mechanism as summarized by Scheme I, eqs 1-11, and Scheme III (with H replacing R).

It is remarkable that the same reaction and mechanism are found starting with metal(II) porphyrins such as Cu(II), Zn(II), and Ni(II) porphyrins as well as with metal(III) porphyrins such as Fe(III) and Co(III) porphyrins. The case of Ni(II) is worth some particular emphasis since the reversible two-electron oxidation wave that has been observed with the Collman picket fence porphyrin (four pivalamido pickets grafted in ortho of each phenyl ring of TPP) has been claimed to yield the corresponding nickel(III) porphyrin cation radical.[4c] It is very likely that this porphyrin follows the same oxidation patterns as the TTPoPiv and a_H-$(C12)_2$-CT-TPP Ni(II) porphyrins investigated here and therefore yields the Ni(II) isoporphyrin along the same mechanism.

In all the examples we have investigated, the internal isoporphyrin formed upon reversible two-electron oxidation of the secondary amide substituted porphyrin shows a further one-electron reversible oxidation wave at higher potentials, similarly to what has been previously observed with exogenous zinc(II) and manganese(II) isoporphyrin.[13b] This was observed for all the secondary amide substituted porphyrins listed in Table I and is shown in Figure 11 in the case of the TTPoPivCu(II) and TTPoPivNi(II) porphyrins. The standard potential corresponding to this wave is not strongly dependent upon the metal (TTPoPivCu(II), 1.550; TTPoPivNi(II), 1.575; TTPoPivFe(III)Cl, 1.700 V vs SCE), indicating that the same type of complex, namely the isoporphyrin dication radical, is likely to be formed in all cases.

Experimental Section

Chemicals. (1) Solvents and Supporting Electrolytes. 1,2-Dichloroethane, methylene chloride, and benzonitrile (Carlo Erba) were distilled over P_2O_5 before use. NBu_4PF_6 was used as supporting electrolyte throughout the present work. It was from commercial origin (Fluka purum) and recrystallized twice in 1,2-dichloroethane and dried under vacuum at 50 °C before use.

(2) Porphyrins. The TPP and a-$(C12)_2$-CT complexes were prepared and characterized according to previously described procedures.[15] The

Scheme VI

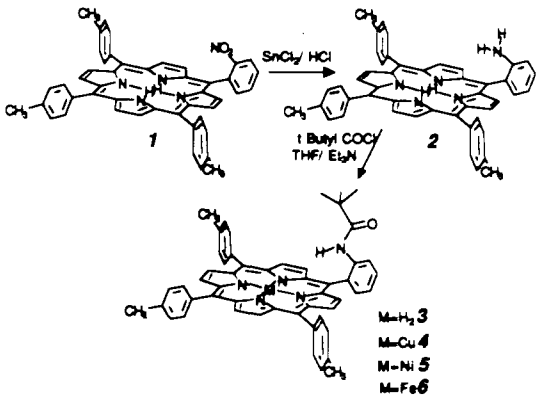

other porphyrins were synthesized as described below.

Chemicals (pyrrole, *p*-tolualdehyde, *o*-nitrobenzaldehyde, pivaloyl chloride) were obtained from Aldrich. Dry tetrahydrofuran (THF) was obtained by distillation from sodium benzophenone and used immediately. Merck silica gel 60 (40–60 μm) was used for column chromatography. Pure porphyrin **2** was obtained by preparative high-pressure liquid chromatography (HPLC) with a Jobin-Yvon instrument. Merck precoated preparative plates (silica gel 60, 2 mm) were used for preparative TLC. Elementary analyses were carried out by the Service de Microanalyse du CNRS.

^{1}H NMR spectra were obtained with a Varian XL100 instrument. Optical spectra in the Soret and visible regions were recorded with a Varian DMS 100 spectrometer.

The mono *o*-nitro-TTPH$_2$ (**1**) was prepared from an appropriate mixture of *p*-tolualdehyde, *o*-nitrobenzaldehyde, and pyrrole (3, 1, and 4 equiv, respectively) by an adaptation of the Adler synthesis,[16] and the monopivalamidophenyl(tritolyl)porphyrin was prepared by an adaptation of the Burckingham method.[17,18] The mixture of two porphyrins [5,10,15,20-(tetratolyl)porphyrin and 5-(*o*-nitrophenyl)-10,15,20-(tritolyl)porphyrin] was used without purification.

The procedure depicted in Scheme VI was followed for the synthesis of the TTPoPivCu and Ni porphyrins.

(a) 5-(*o*-Aminophenyl)-10,15,20-(tritolyl)porphyrin (2). The mixture of 5,10,15,20-(tetratolyl)porphyrin and 5-(*o*-nitrophenyl)-10,15,20-(tritolyl)porphyrin was reduced to the corresponding amino compounds by means of the $SnCl_2$/HCl method[19] followed by chromatography of the crude product on a silica gel column (HPLC) eluted with toluene. The first fraction was (tetratolyl)porphyrin and the second the monosubstituted porphyrin **2**. *o*-Amino-TTPH$_2$ was crystallized from methylene chloride/methanol (1.35% from *o*-nitrobenzaldehyde).

Anal. Calcd for $C_{47}H_{37}N_5$: C, 83.03; H, 5.55; N, 10.42. Found: C, 83.56; H, 5.59, N, 10.59. UV–vis ($CHCl_3$): λ_{max} ($\epsilon \times 10^{-3}$ M^{-1} cm^{-1}) 420.5 (396.9), 517 (18.6), 552.5 (9.3), 591.5 (6.6), 648 (5.5) nm.

(b) 5-(*o*-Pivalamidophenyl)-10,15,20-(tritolyl)porphyrin (3). One hundred milligrams of compound **2** and 0.2 mL of triethylamine in 50 mL of dry THF were reacted, under stirring, with a 10-fold excess of pivaloyl chloride in dry THF. After 1 h, the reaction mixture was evaporated under vacuum and the residue dissolved in methylene chloride. The solution was washed with water,diluted HCl, 0.1 M aqueous $NaHCO_3$, and water and then dried over sodium sulfate. Evaporation to dryness gave a solid residue which was chromatographed on a silica gel plate eluted with toluene. The pure product **3** was collected as one red band and crystallized from methylene chloride/methanol as blue crystals (75 mg, 66%).

Anal. Calcd for $C_{52}H_{45}N_5O$: C, 82.62; H, 6.00; N, 9.26. Found: C, 82.07; H, 5.95; N, 9.25. UV–vis ($CHCl_3$): λ_{max} ($\epsilon \times 10^{-3}$ M^{-1} cm^{-1}) 421 (421.8), 517 (18.3), 552.5 (8.9), 591.5 (6.2), 648 (5.2) nm. ^{1}H NMR ($CDCl_3$): δ 8.89 (s) pyrrole, 8.89 (d) J = 5 Hz pyrrole, 8.77 (d) J = 5 Hz pyrrole, 8.08 (t) tolyl, 8.01 (d) phenyl, 7.58 (d) tolyl, 7.43 (d) phenyl, 7.84 (d) phenyl, 2.72 (s) CH_3, 0.17 (s) *t*-Bu, −2.67 (s) NH.

(c) Copper(II) 5-(*o*-Pivalamidophenyl)-10,15,20-(tritolyl)porphyrin (4).[20] A mixture of 50 mg of compound **3** in 25 mL of chloroform and 100 mg of copper acetate in 5 mL of methanol was refluxed for 30 min. The crude solution was washed three times with water, dried over sodium sulfate, and chromatographed on a silica gel plate with a mixture of toluene/acetone (100:2.5 v/v) as eluent. Fifty milligrams of copper complex **4** was obtained after crystallization from methylene chloride/methanol (95%).

Anal. Calcd for $C_{52}H_{43}N_5OCu$: C, 76.40; H, 5.30; N, 8.57. Found: C, 76.34; H, 5.30; N, 8.87. UV–vis ($CHCl_3$): λ_{max} ($\epsilon \times 10^{-3}$ M^{-1} cm^{-1}) 417 (494.1), 540 (22.7), 576.5 (shoulder) nm.

(d) Nickel(II) 5-(*o*-Pivalamidophenyl)-10,15,20-(tritolyl)porphyrin (5). A mixture of 75 mg of compound **3** in 25 mL of dimethylformamide and 100 mg of nickel acetate in 5 mL of methanol was refluxed for 1 h. The solution was evaporated to dryness, dissolved in methylene chloride, and washed three times with water. After the solution was dried over sodium sulfate and the solvent stripped off by evaporation, the residue was chromatographed on silica gel plate (TLC) eluting with a mixture of toluene/acetone (100:2.5 v/v). Sixty milligrams of nickel complex **5** was obtained after crystallization from methylene chloride/methanol (75%).

Anal. Calcd for $C_{52}H_{43}N_5ONi \cdot 2H_2O$: C, 73.59; H, 5.58; N, 8.25. Found: C, 73.92; H, 5.26; N, 8.38. UV–vis ($CHCl_3$): λ_{max} ($\epsilon \times 10^{-3}$ M^{-1} cm^{-1}) 416.5 (276.5), 529 (19.5) nm.

(e) Iron(III) Chloride 5-(*o*-Pivalamidophenyl)-10,15,20-(tritolyl)-porphyrin (6). A solution of iron(II) chloride in DMF (10 mg/mL) was added to a mixture of compound **3** (50 mg) and 2,6-lutidine (200 μL) in DMF (10 mL) under argon. The solution was heated at 140 °C and stirred until disappearance of free base in UV–visible spectroscopy (2 h). The solution was evaporated under vacuum, dissolved in methylene chloride, washed with water and dried (Na_2SO_4). The crude product was chromatographed on a silica gel plate eluted with methylene chloride/methanol (10:1 v/v). The chloroiron(III) complex dissolved in methylene chloride was generated by shaking with a saturated sodium chloride and HCl (0.1 N) aqueous solution. The porphyrin was used without purification (52 mg, 93%).

UV–vis (toluene): λ_{max} ($\epsilon \times 10^{-3}$ M^{-1} cm^{-1}) 419 (115.6), 511.5 (14.4), 576 (4.5), 657 (3.8) nm.

The a_R–(C12)$_2$–CT–TPPZn porphyrins:

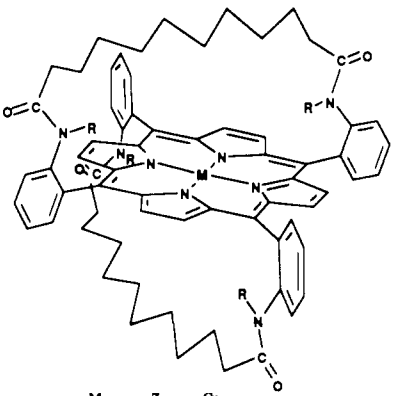

(f) Zinc α-5,α-15:β-10,β-20-Bis[2,2′-(*N*,*N*′-dimethyldodecanediamido)diphenylene]porphyrin (7). A solution of a_H–(C12)$_2$–CT–TPPZn[14,15] (100 mg, 9×10^{-5} mol) in dry dimethylformamide (15 mL) was added dropwise to NaH (200 mg, 50% in oil) at room temperature under argon. After complete addition, methyl iodide was added to the green solution and stirring was continued for 4 h. Solvent was removed on a rotary evaporator, and the residue was dissolved in methylene chloride. The solution was washed with water, aqueous hydrogen carbonate, and water and dried (Na_2SO_4). After evaporation, the residue was chromatographed on a silica gel plate. Elution with dichloromethane/acetone (5:1 v/v) gave a major band (R_f = 0.5) which was identified by NMR spectroscopy as the desired metalloporphyrin **7** (80 mg, 80% after crystallization in dichloromethane/hexane).

Anal. Calcd for $C_{72}H_{76}N_8O_4Zn \cdot H_2O$: C, 72.01; H, 6.55; N, 9.33. Found: C, 71.80; H, 6.56; N, 8.91. UV–vis (CH_2Cl_2): λ_{max} ($\epsilon \times 10^{-3}$ M^{-1} cm^{-1}) 428.5 (416.7), 557 (18.4), 596 (3.9) nm. ^{1}H NMR of the free base **7′** (obtained by acid treatment of **7** with HCl) ($CDCl_3$): δ 8.95 (d),

(15) (a) Momenteau, M.; Mispelter, J.; Loock, B.; Bisagni, E. *J. Chem. Soc., Perkin Trans. 1* **1983**, 189. Momenteau, M.; Mispelter, J.; Loock, B.; Lhoste, J-M. *J. Chem. Soc., Perkin Trans. 1* **1985**, 221.

(16) Adler, A. D.; Longo, F. R.; Finarelli, J. D.; Goldmacher, J.; Assour, J.; Korsakoff, L. *J. Org. Chem.* **1967**, *32*, 476.

(17) Buchinghan, D. A.; Rauchfuss, T. B. *J. Chem. Soc., Chem. Commun.* **1978**, 705.

(18) Walker, A. F.; Balke, V. L.; West, J. T. *Rev. Port. Quim.* **1985**, *27*, 15.

(19) Collman, J. P.; Gagne, R. R.; Reed, C. A.; Halbert, T. R.; Lang, G.; Robinson, W. T. *J. Am. Chem. Soc.* **1975**, *97*, 1427.

(20) Adler, A. D.; Longo, F. R.; Kampas, F.; Kim, J. J. *Inorg. Nucl. Chem.* **1970**, *32*, 2443.

8.71 (s) pyrrole, 7.87 (m), 7.50 (m) phenyl, 2.88 (s) N-CH_3, 2.14 (m), 1.45 (m), 0.31 (m) (CH_2), 2.54 (s), 2.61 (s) NH.

Anal. Calcd for $C_{72}H_{78}N_8O_4$, 1.5 H_2O: C, 75.43; H, 7.12; N, 9.08. Found: C, 75.55; H, 6.91; N, 8.96.

(g) Zinc α-5,α-15:β-10,β-20-Bis[2,2′-(*N*,*N*′-didodecyldodecanediamido)diphenylene]porphyrin (8). A solution of a_H-$(C12)_2$-CT-TPPZn[14,15] (100 mg, 9×10^{-5} mol) in dry dimethylformamide (15 mL) was added dropwise to NaH (200 mg, 50% in oil) at room temperature under argon. After complete addition, dodecyl bromide (0.450 mL, 9×10^{-4} mol) was added to the green solution and stirring was continued for 4 h. Solvent was removed on a rotary evaporator, and the residue was dissolved in methylene chloride. The solution was washed with water, aqueous hydrogen carbonate, and water and dried (Na_2SO_4). After evaporation, the residue was chromatographed on a silica gel plate. Elution with dichloromethane/ether (5:1 v/v) gave a major band (R_f = 0.7) which was identified by NMR spectroscopy as the desired metalloporphyrin **8** (90 mg, 80% after crystallization in dichloromethane/hexane).

Anal. Calcd for $C_{116}H_{164}N_8O_4Zn$: C, 77.4; H, 9.18; N, 6.23. Found: C, 77.45; H, 8.76; N, 5.63. UV-vis (CH_2Cl_2): λ_{max} ($\epsilon \times 10^{-3}$ M^{-1} cm^{-1}) 428.5 (396.7), 520 (shoulder), 557 (19.4), 599 (shoulder) nm. ^1H NMR of free base **8′** (obtained by acid treatment of **8** with HCl) ($CDCl_3$): δ 8.95 (s), 8.65 (m) pyrrole, 7.80 (m) phenyl, 1.20 (m) N-$C_{12}H_{25}$, 1.20 (m), 0.40 (m),0.05 (m) (CH_2), 2.42 (s), 2.30 (s), 2.36 (s) and 2,2.46 (s) NH.

(h) Copper(II) α-5,α-15:β-10,β-20-Bis[2,2′-(*N*,*N*′-dimethyldodecanediamido)diphenylene]porphyrin (9). A mixture of 50 mg of free base **7′** in 25 mL of chloroform and 100 mg of copper acetate in 5 mL of methanol was refluxed for 30 min. The crude solution was washed three times with water, dried over sodium sulfate, and chromatographed on a silica gel plate with a mixture of dichloromethane/acetone (10:1 v/v) as eluant. Fifty milligrams of copper complex **8** was obtained after crystallization from methylene chloride/hexane (95%).

Anal. Calcd for $C_{72}H_{76}N_8O_4Cu$: C, 73.23; H, 6.49; N, 9.49. Found: C, 72.96; H, 6.5649; N, 9.23. UV-vis ($CHCl_3$): λ_{max} ($\epsilon \times 10^{-3}$ M^{-1} cm^{-1}) 418 (490), 540 (21), 576 (shoulder) nm.

(i) Copper(II) α-5,α-15:β-10,β-20-Bis[2,2′-(*N*,*N*′-didodecyldodecanediamido)diphenylene]porphyrin (10). A mixture of 50 mg of free base **8′** in 25 mL of chloroform and 100 mg of copper acetate in 5 mL of methanol was refluxed for 30 min. The crude solution was washed three times with water, dried over sodium sulfate, and chromatographed on a silica gel plate with a mixture of dichloromethane/acetone (10:1 v/v) as eluant. Fifty-one milligrams of copper complex **10** was obtained after crystallization from methylene chloride/hexane (95%).

Anal. Calcd for $C_{116}H_{164}N_8O_4Cu$: C, 77.48; H, 9.19; N, 6.03. Found: C, 77.23; H, 9.49; N, 5.98. UV-vis ($CHCl_3$): λ_{max} ($\epsilon \times 10^{-3}$ M^{-1} cm^{-1}) 418 (465), 540 (19.5), 576 (shoulder) nm.

Electrochemical Instrumentation. The cells, instruments, and procedures used for cyclic voltammetry and thin-layer UV-vis spectroelectrochemistry were the same as previously described.[21] The UV-vis-near-IR spectra were recorded on a Varian 2300 spectrophotometer. The working electrodes were a 3 mm diameter glassy carbon disk in cyclic voltammetry and a 2.4 cm^2 platinum grid in spectroelectrochemistry. The reference electrode was a Ag/0.1 M $AgClO_4$ in benzonitrile, 400 mV positive to the saturated calomel electrode to which all potentials are referred throughout this paper. A platinum grid electrode was also used in the thin-layer FTIR experiments. It was sandwiched between two CaF_2 windows, and the absorption was measured by transmittance.

Conclusion

It is remarkable that all NHCO-containing basket-handle and picket porphyrins investigated in this work display a reversible two-electron–one-proton oxidation reduction behavior whatever the nature of the central metallic ion, Cu^{2+}, Zn^{2+}, Ni^{2+}, Fe^{3+}, Co^{3+}.

The essential mechanistic ingredients that make the system reversible are the following. An endogenous isoporphyrin complex is formed at the level of the porphyrin dication by expulsion of the secondary amide proton and formation of an oxazoline ring that involves the deprotonated amide and the neighboring meso carbon of the porphyrin ring. The appearance of a two-electron oxidation requires that this chemical transformation possesses a substantial driving force to drive the otherwise downhill disproportionation of two porphyrin cation radicals. However, the appearance of a two-electron reduction of the isoporphyrin cation thus formed requires that this driving force be not too large and that a nonnegligible amount of the protonated isoporphyrin dication be present at equilibrium so as to allow an efficient autocatalysis of the reduction. The reversibility of this two-electron–one-proton ring closure/opening process is thus the result of a delicate balance between the driving forces offered by these various steps in both directions. Such a balance is not achieved in the tertiary amide case, although an isoporphyrin is also formed and in spite of the fact that its reduction is a two-electron reaction due to the same autocatalytic process. The oxidation, however, involves the stepwise removal of the two electrons because the driving force offered by the ring closure step is not sufficient to drive the cation radical disproportionation to completion. Recent observation of a two-electron oxidation process, with secondary amide substituted porphyrins where a CONH group instead of a NHCO group is attached to the ortho positions of the phenyl rings of TPP, although less reversible than with the NHCO-substituted porphyrin, most probably also involves the formation of an internal isoporphyrin complex.[22] The isoporphyrin would then contain a five- instead of a six-membered ring.

Acknowledgment. A. Croisy (Institut Curie, Orsay, France) is thanked for his help in designing the IR cell. M. Simon (Itodys, Université de Paris 7), A. Lautié (Lasir, Thiais, France), and G. Calas (Laboratoire de Minéralogie de l'Université de Paris 7) are gratefully thanked for the permission to use their IR and near-IR instruments and their helpful advice in the interpretation of spectra.

Registry No. 2, 131352-79-9; **3**, 131352-78-8; **4**, 131352-97-1; **5**, 131352-96-0; **5**$^+$, 131352-94-8; **6**, 131352-95-9; **6**$^+$, 131352-93-7; **7**, 131352-92-6; **7**$^+$, 131352-89-1; **7**$^{2+}$, 131352-90-4; **9**, 131352-81-3; **9**$^+$, 131352-84-6; **9**$^{2+}$, 131352-85-7; **10**, 131352-80-2; **10**$^+$, 131352-86-8; **10**$^{2+}$, 131352-87-9; TTPoPiv, 131352-78-8; a_H-$(C12)_2$-CT-TPP, 98360-58-8; IP$^+$ (M = Cu), 131352-98-2; IP$^+$ (M = Ni), 131352-99-3; CF_3CO_2H, 76-05-1; Cu-a_H-$(C12)_2$-CT-TPP, 91900-02-6; Cu-a_H-$(C12)_2$-CT-TPP$^+$, 131352-83-5; CuTPP, 14172-91-9; CuTPP$^+$, 28206-02-2; CuTPP^{2+}, 28132-68-5; Zn-a_H-$(C12)_2$-CT-TPP, 91928-44-8; Zn-a_H-$(C12)_2$-CT-TPP$^+$, 131352-88-0; ZnTPP, 14074-80-7; ZnTPP$^+$, 39732-73-5; ZnTPP^{2+}, 21558-86-1; Ni-a_H-$(C12)_2$-CT-TPP, 117688-00-3; Ni-a_H-$(C12)_2$-CT-TPP$^+$, 131352-91-5; NiTPP, 14172-92-0; NiTPP$^+$, 29484-62-6; NiTPP^{2+}, 57208-12-5; Fe-a_H-$(C12)_2$-CT-TPP$^+$, 93646-93-6; Fe-a_H-$(C12)_2$-CT-TPP^{2+}, 93646-94-7; FeTPP$^+$, 29484-63-7; FeTPP^{2+}, 28132-70-9; FeTPP^{3+}, 129149-02-6; Co-a_H-$(C12)_2$-CT-TPP$^+$, 111902-97-7; Co-a_H-$(C12)_2$-CT-TPP^{2+}, 131352-82-4; CoTPP$^+$, 38414-01-6; CoTPP^{2+}, 28132-69-6; CoTPP^{3+}, 60430-19-5; pivaloyl chloride, 3282-30-2; methyl iodide, 74-88-4; dodecyl bromide, 143-15-7; 2,6-lutidine, 108-48-5.

(21) Lexa, D.; Savéant, J-M.; Zickler, J. *J. Am. Chem. Soc.* **1977**, *99*, 786.

(22) Leondiadis, L.; Momenteau, M. *J. Org. Chem.* **1989**, *54*, 6135.